Jia, Ke and Bi, Tianshu and Ren, Zhefeng and Thomas, David W.P. and Sumner, M. (2018) High frequency impedance based fault location in distribution system with DGs. IEEE Transactions on Smart Grid, 9 (2). pp. 807-816. ISSN 1949-3061

High frequency impedance based fault location in distribution system with DGs

K. Jia, T.S. Bi, Zhefeng Ren, D.W.P Thomas and M. Sumner

***Abstract*— Distributed Generations (DGs) with power electronic devices and their control loops will cause distortion to the fault currents and result in errors for power frequency measurement based fault locations. This might jeopardize the distribution system fault restoration and reduce the grid resilience. The proposed method uses high frequency (up to 3kHz) fault information and short window measurement to avoid the influence of DG control loops. Applying the DG high frequency impedance model, faults can be accurately located by measuring the system high frequency line reactance. Assisted with the DG side recorded unsynchronized data, this method can be employed to distribution systems with multiple branches and laterals.**

***Index Terms*-- fault location, high frequency transient, distribution systems.**

I. Introduction

Economical, political, environmental, societal and technical factors have driven the installation of distributed energy resources in distribution systems [1]. With pre-designed controls, embedded Distributed Generations (DGs) can reduce the energy transmission/distribution losses. The network survivability and resilience can be improved by providing continuous energy supply to the local loads from DGs in case of the main system faults [2]. However, compared with the conventional synchronous generators, DGs (such as the wind power and PV generations) can only provide limited fault currents and unique fault transient characteristics due to the applied power electronics and control logics. Currently, the correct operation of the conventional protections and fault location systems are challenged by this distorted fault current from DGs. When the DG installation volume is small (not considered as a factor that would influence the system power utilization efficiency), instead of re-design the fault location and protection algorithms, DGs are disconnected from the grid during a fault to achieve a correct operation of the relays and fault locations that are designed based on single power source. With fast increased installation volume of the DGs [3], disconnecting all the DGs during a fault would influence the power generation efficiency. New fault location algorithms that consider the existence of DGs are required.

Fault locations in the distribution system have been investigated for decades and can be classified into four groups: the system frequency impedance estimation based method, the traveling wave method, the injection based method and the wide-area measurement based method.

This work was supported in part by the National program on key basic research project (973 Program, No. 2012CB215206), by the NSFC project under Grant 51407067, the "111" Project under Grant B08013.

In [4] and [5], the single-ended technique based on measured pre-fault and post fault information is developed by Takagi. Then Srinivasan, Girgins, Zhu, Das, Choi, Lee, Florez, Salim, and Nouri have modified and extended the impedance based method. This type of fault location has to deal with three unknown variables: the fault distance, the fault resistance and the load current. The unknown fault resistance can be eliminated by using both the real and imaginary equations or involving the negative sequence current [6-8]. The load current is assumed to be equal to its pre-fault value and the iteration is used to cancel the error [8][9]. When considering the three unknown variables at the same time, the load impedance is normally assumed to be a known value derived from the pre-fault load flow calculation [10-15] or not considered for some cases [16-17]. The single-ended impedance based methods are more attractive for industry applications due to the straight forward algorithm and lack of a communication channel. They can be extended and applied to the main distribution lines with tapped loads (initially assuming the fault is in the first sections and then carry on to the next sections).

For a large distribution system (especially the one with a large number of connection nodes), locating a fault from single-ended measurement is challenging. In this case, the wide area measurement based location is developed due to the increase installation of the Intelligent Electronic Devices (IEDs) in the distribution systems. Instead of the impedance estimation, the voltage and current variations (voltage sag or current increase) are directly captured to locate faults. The voltage sag based fault location is firstly proposed by Galijasevic and Abur [18] and extended by Pereira [19], Xu[20] and other researchers[21-23]. This method uses the pre-fault and post-fault steady state voltage to calculate the amplitude sags in different fault scenarios. The fault is located by comparing the pre-calculated patterns with the measured values. For some cases, the pre-fault current, phase angle and fault type information are also used to increase the fault location accuracy [21]. The adaptive neuro-fuzzy inference system and artificial neural network [22], Decision-tree [23], Primal-dual interior point and the log barrier algorithm [24-25] are used for precise pattern recognition. This method is suitable for all networks when the measurements from all (or most of) the nodes are available. But the intelligent pattern recognition algorithms might take a long time at current data processing speeds and it is difficult to fully specify the training set.

Compared with other methods, traveling wave (or the

frequency characteristics of traveling waves) and injection based methods can provide fast and accurate fault location but require high frequency data acquisition units and injections. The traveling wave method can locate faults with an error of a few metres for a sampling frequency from kHz up to 1MHz [26-27] in different system topologies. However, traveling waves propagate at the speed of the light, so it is challenging to capture the wave fronts when fault is close to the measurement point and this leads to a close-end "dead zone". On distribution systems it requires far more processing than the transmission system because of the reflected waves from the many laterals [29]. The traveling wave frequency methods use wavelets to capture the transient characteristics as the characteristic frequency will be lower for more distant faults [30][31]. Compared with the direct traveling wave algorithm, frequency based methods require a lower sampling frequency but still has the close-end "dead zone". The injection based method injects high frequency transients or harmonics to the system and measures the responses to locate the fault. For different fault locations, the responses are normally unique. It was originally designed for off-line cable fault location [32-34] and then developed for over-head line fault location [35-36]. However, the injection unit cannot be available for all the systems and it might influence the system healthy operation during online fault locations.

Considering the penetration of DGs, the introduced fault location methods mostly use the system frequency impedance [37-38] and voltage sag calculation [39-40]. In these papers, the DG is considered as a voltage source that can alter the load flow directions and still provide sinusoidal wave forms after fault occurs [41]. However, most of the DGs are connected to the grid with the assistance of the power electronics and are not able to provide enough grid voltage support during a fault. DGs are normally controlled to inject power to the system while the grid provides constant voltage support. During an un-symmetrical fault, the symmetrical control design can lead to negative sequence frequency injection from the DG. In this case, seen from the DG side, the system positive and negative sequence impedance is not equal. Also, the grid side voltage drop (caused by faults) will induce currents to rise in the inner control loops and this leads to large non-sinusoidal and low frequency distortion outputs from DGs. Considering the control loops and the power electronics, the DGs cannot be linearly represented for fault location based on system frequency data measurement. The non-sinusoidal and low frequency distortion output from DGs will cause errors to the system frequency measurements as well.

This paper introduces a high frequency (up to 3kHz) impedance measurement based fault location for the distribution system with DGs. The main contributions of this paper are: 1) A high frequency impedance based DG model is developed for fault location regardless of its control loop influences. 2) A fault transient measurement based fault location is provided. Using short data capturing window and system high frequency impedance, both the speed and accuracy of the fault location can be improved. 3) With the assistance of the DG side measurements (such as measurements used for islanding protections), the proposed algorithms can have a good accuracy in the distribution system with multiple laterals.

II. Algorithm Overviews

A. High frequency impedance based fault location

It is recognized that a short circuit fault acts as a step voltage transient from the point of fault inception, and therefore, contains wideband frequency information [30][31]. The high frequency fault transients can be picked out and transformed into the frequency domain by continuous wavelet methods [37] and the fault location can be fixed by calculating the high frequency line impedance from the measurement point to the fault. This paper focuses on locating faults with enlarged fault currents such as phase to phase faults or phase to ground faults in an uncompensated distribution system. High impedance faults and ground faults in a compensated system are not considered.

1) Zero fault impedance situation

The proposed fault location method can be demonstrated using the equivalent two-generator system as shown in the Fig.1 with a metallic fault (the fault resistance is ignored).

In the Fig.1 (a), Z_S is the [3x1] three phase source impedance matrix, Z_R is the [3x1] three phase remote-end impedance matrix, Z_{line_P} is the [3x3] per-unit length line impedance, x_f is the fault distance from the measurement point and the L is the length of total distribution line. From superposition theory for a short circuit fault, the fault transient can be treated as a voltage step at the fault point and creates an equal and opposite voltage to the instantaneous pre-fault voltage $V_{pre\text{-}f}$ at the fault location. This step waveform created by the fault can be considered as a high frequency signal source at the fault location (step waveform will have energy throughout the frequency range of interest after being transferred in to the frequency domain) as shown in the Fig.1 (b).

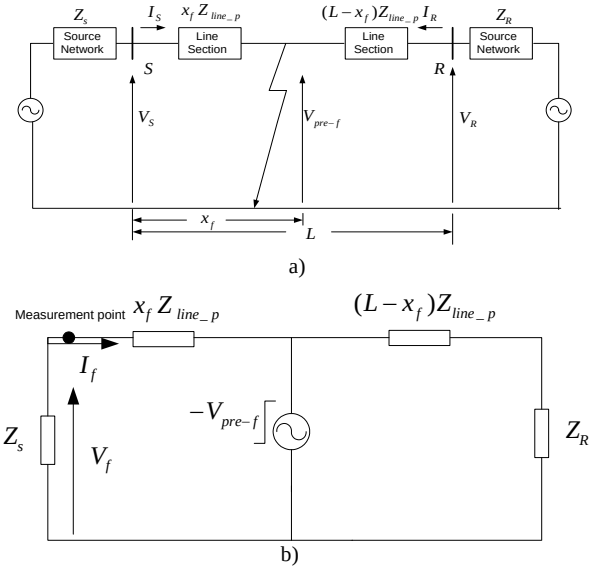

Fig. 1 (a) Equivalent faulted system at power frequency. (b) Equivalent system circuit for high frequency transients.

The source impedance can be directly calculated using the high frequency transient measured at the measurement point. The total source and line impedances can then be found in terms of the fault transient voltage at the fault location $V_{pre\text{-}f}$ (a three phase [3x1] matrix) and the measured transient current I_f (a three phase [3x1] matrix).

$$Z_s + Z_{line\_P} x_f = \frac{V_{pre-f}}{I_f} \tag{1}$$

Thus the line impedance between the measurement point and the fault location can be obtained.

$$Z_{line\_P} x_f = \frac{V_{pre-f}}{I_f} - \frac{V_f}{I_f} \tag{2}$$

In this location scheme, $V_{pre\text{-}f}$ is initially assumed to be equal to the healthy state voltage at the measurement point. This will lead to an initial error in the fault distance estimation.

This error in the fault location measurement is due to the difference between the pre-fault voltage at the measuring point ($V_{pre\text{-}f}$) and the actual pre-fault steady state voltage at the fault location ($V'_{pre\text{-}f}$) as described in (3). This $V'_{pre\text{-}f}$ can be used to create the step fault transient for further iterations.

$$V'_{pre-f} = V_{pre-f} - I_{pre} Z_{line\_P} x_f \tag{3}$$

Initially the fault location and fault resistance will be unknown. However, an initial estimation can be carried out from the imaginary part of (2) as it is independent of the fault resistance (noted that for frequencies greater than system frequency, this is not affected by the remote in-feed). The fault location is then estimated from:

$$x_f = \frac{imag(\frac{V_{pre-f}}{I_f} - \frac{V_f}{I_f})}{imag(Z_{line\_P})} \tag{4}$$

The fault distance (x_f) initially derived by (4) has an error due to the approximation of the pre-fault voltage. This fault distance is then used in (3) to compensate the pre-fault voltage estimation errors. For a converging iteration the calculated Δx between two iterations is a decreasing value. If necessary this iteration is repeated and the pre-fault voltage at the fault location can be compensated until the fault location error converges to within a reasonable tolerance. The following equations (5)-(8) explain the iteration converging process.

For n+1 iteration:

$$x_{n+1} X_{line\_P} = \frac{V_{pre-f} - I_{pre} X_{line\_P} x_n}{I_f} - \frac{V_f}{I_f} \tag{5}$$

where $X_{line\text{-}p}$ is the line reactance per unit length (the high frequency reactance dominates the impedance value and the line resistance is ignored for simplification). x_{n+1} and x_n are estimated fault distance for n+1 and n iterations.

Let $x_n = x + \Delta x$ and if the estimated x is the real fault distance and when $\Delta x = 0$:

$$I_{pre} X_{line\_P} x = -I_f X_{line\_P} x + V_{pre} - V_f \tag{6}$$

For $x_n = x + \Delta x$ then we have:

$$x_{n+1} = \frac{V_{pre} - I_{pre} X_{line\_P} (x_n + \Delta x)}{I_f X_{line\_P}} - \frac{V_f}{I_f X_{line\_P}} \tag{7}$$

Sub (6) to (7)

$$x_{n+1} = x_n - \frac{I_{pre}}{I_f} \Delta x \tag{8}$$

It shows that the iteration will always converge if the fault current (I_f) is larger than the steady state current (I_{pre}) and this is true for most of the fault situations considered in this work.

2) *Considering fault impedance*

Considering the fault resistance, the line resistance is small compared with the fault resistance and the majority error in the fault location is not caused by the voltage drop from voltage measurement point to fault point but by the fault resistance being comparable to the load impedance. The high frequency system equivalent circuit is shown in the Fig.2.

For this system where the fault impedance cannot be ignored, (3) is modified as below:

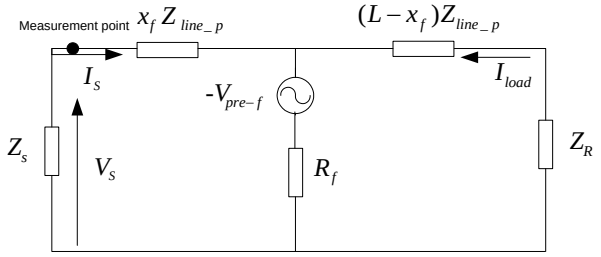

Fig. 2 Equivalent high frequency system with fault resistance.

$$Z_{line\_P} x_f = \frac{V_{pre-f}}{I_s} - R_f - \frac{V_s}{I_s} - \frac{I_{load}}{I_s} R_f \tag{9}$$

The total impedance Z_T which includes the total line impedance and the load impedance can be estimated using the pre-fault steady state data at the measurement point:

$$Z_T = Z_{line\_T} + Z_R \tag{10}$$

The load impedance contains the passive load and the equivalent impedance of the DGs in the high frequency domain. The passive load impedance can be monitored in the distribution system by the installed IEDs and updated by minutes (assuming the passive load remain unchanged during the update intervals). It is then converted into high frequency domain for calculation (the passive load impedance has linear performance within the frequency of interest). The equivalent impedance of the DGs can vary during a fault due to its control (fault current can be influenced by the control loops) and the high frequency impedance model of the DG is discussed in the latter part of this section.

The load current I_{load} is related to the source current I_s for a given fault distance x_f by:

$$\left.\begin{aligned} I_{load=} I_s \frac{Z_S + x_f Z_{line\_P}}{Z_T - x_f Z_{line\_P}} \\ Z_s = \frac{V_s}{I_s} \end{aligned}\right\} \tag{11}$$

And the fault resistance can be calculated as:

$$R_f = \frac{V_{pre-f} - V_S - I_s X_{line\_P} x_f}{I_s + I_{laod}} \tag{12}$$

The iteration procedure can be carried out with (9)-(12) which includes the pre-fault steady state and the fault transient state calculations. The fault distance and the fault resistance can be estimated at the same time. However, for an extremely large fault resistance, the fault transient can be attenuated and this would lead to a poor signal to noise ratio (SNR) and errors in the estimated results. This will be discussed in the simulation results.

3) Considering multiple loads/DGs

Distribution systems normally have multiple branches for loads and DGs connections. Accurate fault location can be achieved if measured at the terminals which are close to the fault and most importantly without any load/DG branches in between as discussed. The load and DG branches between the measurement point and the fault point can be paths for the high frequency fault current and result in errors for the fault location. For a distribution system with tapped loads, in the fault high frequency, the system configuration with multiple "T" connections is shown as in the Fig.3.

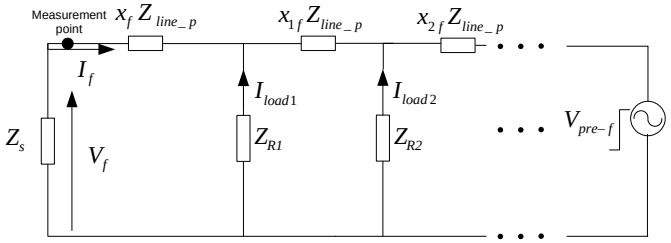

Fig. 3 The distribution system with multiple laterals in high frequency

For the described system, the (4) can be rewritten as:

$$x_f + (1+\frac{I_{load1}}{I_f})x_{1f} + (1+\frac{I_{load1}+I_{load2}}{I_f})x_{2f} .... + (1+\frac{\sum_{n=1}^{N} I_{loadn}}{I_f})x_{Nf} = imag(\frac{V_{pre-f}}{I_f} - \frac{V_f}{I_f}) / imag(Z_{line\_P}) \quad (13)$$

In (13), N indicates the total number of the "T" connected braches. The relationship between measured high frequency fault current (I_f) and the load high frequency current (I_{load}) can be approximately represented by the source and the load impedances.

As described in (14), the load side current can be approximately represented by the updated load impedance information and the source impedance. The iteration calculation starts from the first section (assuming the fault is in the middle of the first line section and the values of x_{1f}, x_{2f}...x_{nf} are set to be zero).

$$\left.\begin{aligned} I_{load1} / I_f &= Z_s / Z_{load1} \\ \sum_{n=1}^{N} I_{loadn} / I_f &= Z_s / \sum_{n=1}^{N} Z_{loadn} \end{aligned}\right\} \quad (14)$$

If the actual fault is in the further sections the iteration process will not converge (the estimated distance value increases with iterations) and the x_{1f} is considered. Then the x_{2f} and other further sections can be considered until the iteration converges.

However, this process might require load side measurements and a long data processing time for systems that have other than "T" connections. Also, the approximating representation in (13) and (14) can lead to enlarged errors in fault location results with the increase of fault distance. In this case, if the load side measurements are available the (13) and (14) are used. For practical consideration, only the DG and the main grid side measurements are used. This might lead to errors in the exact fault distance estimation but the faulted line section can still be distinguished and isolated.

For description convenience, the name fault location unit (FLU) which uses the system and DG side grid connected protection (required when the DG is connected to the grid) measurement data is employed in this paper. For practical utilization, the FLU can be an embedded function within the DG islanding protections and uses the recorded voltage and current data. One set of FLU cannot cover the entire distribution system and this is especially true for system with multi-laterals and branches. However, if the FLUs are not only installed at the substation buses but also at the DG side, this problem can be addressed using the wide area measurement. The relationship of (13) can be rewritten as:

$$x_f + (1+\Delta 1)x_{1f} + (1+\Delta 2)x_{2f} .... + (1+\Delta n)x_{Nf} = imag(\frac{V_{pre-f}}{I_f} - \frac{V_f}{I_f}) / imag(Z_{line\_P}) \quad (15)$$

The value of Δ in (15) is small and can be treated as errors which increase with fault distances due to the fact that the load impedance is normally much larger than the system source impedance. In a system with multi-FLUs, for the first step calculation, the previous discussed algorithm using (1)-(12) is used (laterals are not considered). Although each of the FLU might have fault location errors, the comparable ratio of the all the fault location results can be used to select the faulted sections and then (13) and (14) are only used for the exact fault distance estimation if necessary. The FLU which shows the shortest estimated distance will give the most accurate result. In cases where faults on different branches might have the same distance to the closest FLUs. The ratio of the second and the third shortest fault location results from the other FLUs will be helpful during the actual fault distance distinguishing process. In this situation, the un-synchronised wide-area measurement is required and only the results of each of the FLUs are communicated.

B. High frequency impedance model of DFIG

DGs can be classified into two groups: the directly grid connected one as the Double Fed Induction Generator (DFIG) as shown in the Fig.4 and the inverter connected as PV and fuel cells. This paper will focus on the directly grid connected DGs and the model of the other type of DGs will be discussed in the next paper.

The DFIG relies on the grid side voltage for the rotor excitation through back to back AC/DC converters. Once the grid side voltage drops (during a shot circuit fault) are detected the rotor side controller tries to generate more current to balance the detected stator side phase angle differences. This

can result in variable equivalent impedance during a fault. To make the matter worse, the control design for each control loops (inner loops, outer loops, phase lock loops, etc.) are unique for different manufactures. Also, sometimes the rotor side crowbar and DC bus Chopper protection are tripped when large rotor current or DC voltage increases are detected during the fault. All the mentioned phenomenon leads to an almost unsolvable question for the precise DFIG fault current calculation. Considering the control mutual influences between multiple DFIGs, it is impossible to build a precise impedance model which is suitable for all the DFIGs for the protection and fault location based on power frequency measurement.

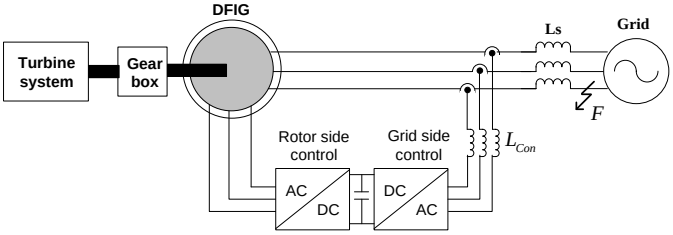

Fig. 4 Configuration of DFIG wind power system

However, in the high frequency domain, the common impedance model for all DFIGs can be derived. The proposed fault location method uses only the high frequency fault transients and the pre-fault data. During a fault, only several ms of fault transients (6 ms after the fault occurs) are used. The DFIG control response time is about several tens to hundreds ms which mainly depends on design of the PLL, inner and outer control loops. In this time period, the influences caused by different control loop designs can be ignored due to the fact that the response time is much larger than the data capture window. In this case, the DFIGs can be modeled as high frequency induction motor impedance which is paralleled with its control circuit impedance as shown in the Fig. 5.

As shown in the Fig.5, the R_s, L_s, R_r and L_r are the stator and rotor side equivalent resistance and inductance, the L_m is the motor magnetizing inductance, the L_{Con} is the stator side converter inductance (chock filtering inductance) and the C is the DC link capacitance. For the highly inductive system (cables, transformers and motors) considered in this paper, the best SNR will be at relative low frequencies. A high frequency range up to 3kHz is chosen to a) get good SNR, b) be within the bandwidth of standard current and voltage transducers (have a linear performance within 3kHz) used for this type of operation, c) to restrict sample frequencies to those standard data acquisition equipment (such as the A/Ds on the DSP boards). In this frequency range, the system parasitic capacitance effects can be ignored.

For the common DFIG model as shown in the Fig.4, in the frequency domain (higher than the switching frequency), if the switching state of the IGBT is not considered the converter is equivalent as a short circuit. In this case, the DFIG equivalent model is the induction motor (impedance) in paralleled with the L_{Con} (the inductor within the excitation loop).

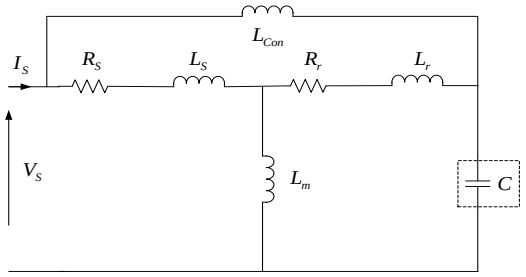

Fig. 5 High frequency model of DFIG

However, when considering the switching states (idea switches), the equivalent impedance part in the dashed rectangular box is either the DC link capacitor or a short circuit. Due to the fact that a large DC link capacitor is employed in practice, then the equivalent impedance differences between the capacitor and the short circuit can be small in the high frequency range and can be treated as one model. The proposed DFIG high frequency model is further tested and validated using the simulation results.

The basic DFIG model (such as the GE model [24]) that has an induction generator, back to back AC/DC/AC converters and filters (as shown in Fig.4) is commonly used for research [42-45]. The lately modifications of the DFIG are mainly to provide the low voltage fault ride through (LVFR) ability [43-45]. The crowbar (and/or copper) control circuits have been added in the hardware [44]. In the control part, current models from ABB and ALSTOM are equipped with positive and negative control algorithm and can generate reactive currents when the system voltage is lower than certain threshold for better LVFR [45]. For system frequency modeling, the control algorithms which might change for different system operating conditions have to be considered. However, this paper only focuses on the high frequency model of DG, in which the control response time is longer than the captured transients and can be ignored. Considering this, the DFIG with alternative control algorithms will not cause differences. The crowbar circuit operations depend on the different fault conditions. When crowbar is switched on, the converters are bypassed and the DFIG can be modeled as an induction generation as shown in Fig.5 in both the system frequency and the high frequency. In this case, the crowbar operation is not a problem for the provided model.

III. Simulation Results

A. Results of DFIG impedance modeling

The introduced high frequency impedance model of DFIG is validated using a GE 1.5MW Wind Turbine-Generators for both online and offline tests. A triangular current transient which has the similar frequency domain performance as a fault transient is used and injected to the DFIG during grid connection (online) and de-energized (offline) operations. The measured time domain data is shown in the Fig. 6.

The data is captured by a short rectangular window (12ms in total length and 6ms after injection) with a 50kHz sampling frequency. This sampling frequency can provide results with

good SNR in the interested frequency range and also is within the data processing limitation of a practical signal processing board. The captured data is filtered (with a cut-off frequency of 4kHz) and then transformed into frequency domain using a modified continuous Morlet wavelet method [46] which is more suitable for picking out the non-sinusoidal transients:

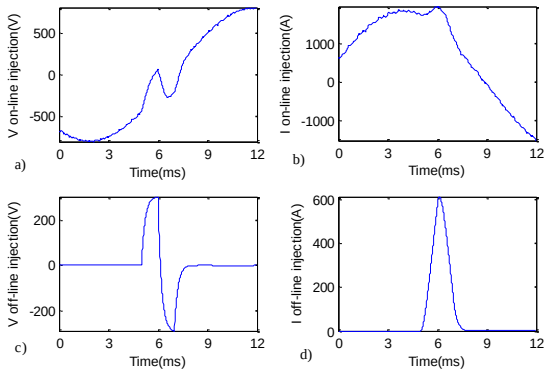

Fig. 6 Measured voltage and current for online and offline tests. a) voltage for online test. b) current for online test. c) voltage for offline test. d) current for offline test.

$$\varphi(x) = \frac{1}{\sqrt{\pi f_b}} e^{j2\pi f_c x} e^{\frac{-x^2}{f_b}} \tag{16}$$

where the bandwidth frequency f_b is 10Hz and the centre frequency f_c is 2kHz to emphasize the accuracy of the results in the interested frequency range. The measured impedances in the frequency domain are shown as in the Fig. 7.

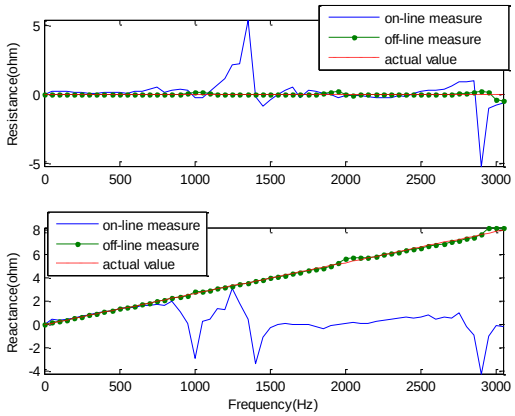

Fig.7 Calculated impedance for the high frequency DFIG model

As shown in the Fig.7, the measured on-line and off-line impedances are plotted against the actual value (dashed red lines). The reactance part shows that off-line test results match with the actual value and are not influenced by the converter transients and the system power frequency leakage. Due to a relatively small resistance value in the frequency domain, the resistance estimation has larger errors and only the reactance model is accurate enough for fault location.

Due to a short window, the edges of the captured data in the time domain can cause disruption in the frequency domain (if not carefully processed, the frequency domain information induced by those edges can be mixed with the injection/fault transient information). This influence is especially obvious in the higher frequency part (above 1kHz). In this case, the lower frequency range results (500Hz to 1kHz) can still be curve fitted and used for modelling the DFIGs. Assuming the DFIG impedance model has a linear performance in the frequency domain of interest, the full frequency domain (up to 3kHz) model can be represented using the accurate estimated lower frequency results.

B. Results of fault location

The proposed fault location scheme is further tested and demonstrated using Matlab simulation results. The IEEE 33 node distribution system [47] (modified with DGs) is used and shown in the Fig. 8.

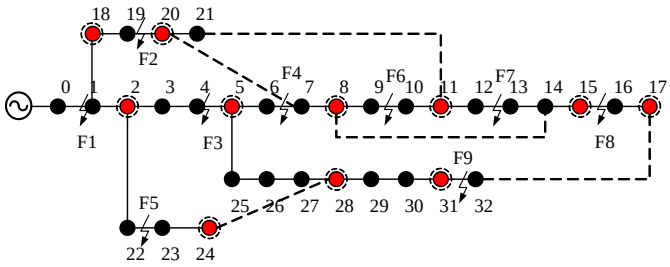

Fig.8 Configuration of the tested distribution system with DFIGs

As shown in Fig. 8, the 11kV system contains DGs, loads and different lengths of lines. The red nodes with dashed circles indicate modified 0.5MW DFIGs (added with crowbar circuit) and the rest nodes are connected with loads. In practice, the dashed lines are normally disconnected in healthy systems to avoid close-loop operations. Detailed information about the system parameters are provided in Table1-Table2 in the Appendix. Nine faults are randomly placed at the start, the middle and the end of the faulted line sections. FLUs are installed at the 11kV substation bus and each of the DGs. For the initial test, a phase to ground fault with a 1Ω resistor is imposed at a distance of 10km to the distribution bus (F1). The measured three phase voltages and currents fault transients are shown in the Fig.9

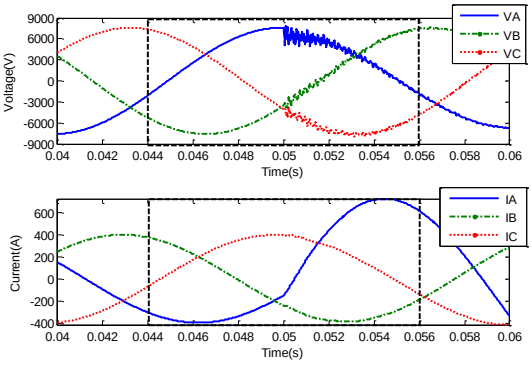

Fig.9 Measured fault voltage and current transients

One cycle data which includes pre-fault & post-fault steady state and the fault transient is plotted. The actual data used for fault location is the one within the dashed rectangular window. Only 6ms of the post-fault transients (less than the DFIG control response time) are included in the window.

Using the short-window high frequency transient data at the terminal of the 11kV distribution bus, the fault distance can be estimated with the iteration process as shown in the Fig.10.

For a fault at 10km, the estimated distances for 7 iterations in the frequency domain are shown in the Fig.10. The error of is reduced in the iterations and within required tolerance (when difference between previous and the current calculation is less than 2%) after the 7th iteration. With the iteration continuing, the estimated steady state voltage $V'_{pre\text{-}f}$ at the fault point shows smaller errors compared the actual fault point step voltage as shown in the Fig.11

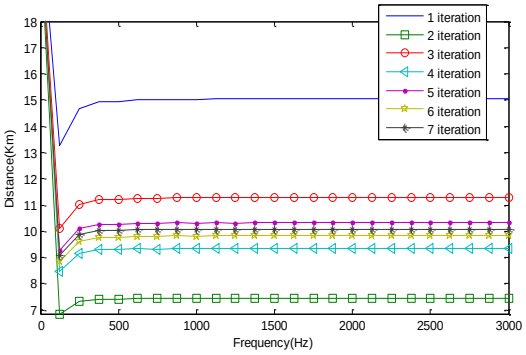

Fig.10 Calculated fault distance for each iteration procedure

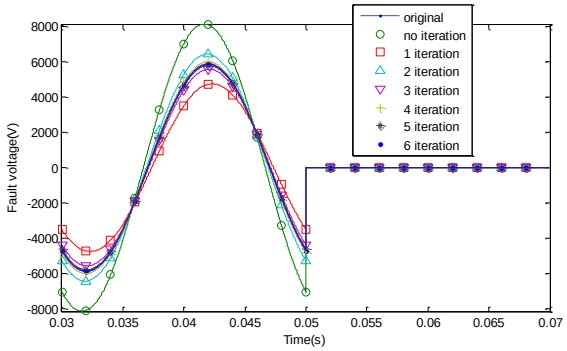

Fig.11 Estimated fault point step voltages for each iteration procedure

C. Influence of the fault impedance

Ideally, the fault resistance is considered in the fault location algorithm and its value can be calculated during the procedure. However, large fault resistance can result in small fault transients (especially in the measured fault current transients) and this could lead to poor SNR and enlarged errors in the estimated results. With the inclusion of a constant percentage of 1% background noise (40dB white noise generated by the MATLAB band-limited white noise function), for a fixed fault distance, the estimated errors increase with the fault resistance as shown in Fig. 12.

As shown in Fig.12, the Z_{load} is the largest load impedance. Fault location error reaches the maximum allowable value (about 5%) when the ratio of fault resistance over the rms value of the largest load impedance is about 20%. Fault location error increases significantly after that point due to a smaller fault transient (poor SNR) caused by the enlarged fault resistance. The error can be 120% and even higher when the fault resistance is comparable with the load impedance. In this case, the fault behaves similarly as the load variation and is challenging for detection. This extremely large error is mainly caused by the fact that the iteration calculation may not be converging when the fault resistance value and the load impedance are comparable as discussed in (8).

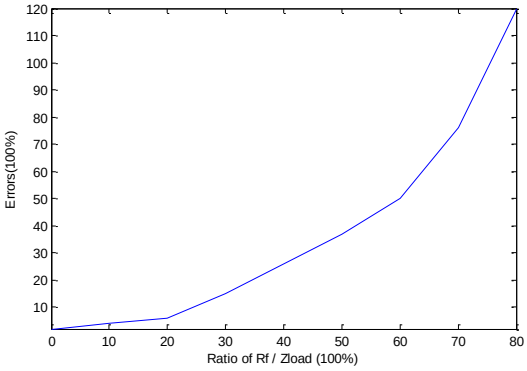

Fig.12 Estimated fault location errors against the fault resistance

Besides the fault impedance the fault inception angle can results in small fault current transients as well. Theoretically, when fault occurs at the zero degree fault inception angle, high frequency transients do not exist. Considering the background noise and the iteration errors, faults with inception angle close to zero (poor SNR) can lead to larger errors in the location. Through multiple tests, range of this fault inception angle is within $\pm 6^{o}$. Within this zone, the fault location results are not used. However, in practical systems, most of the fault occurs at the high fault inception angles (close to $\pm 90^{o}$). Even when the short circuit fault occurs at the 0^{o}, due to low arc energy, the insulation of the line/cable will not be destroyed. The actual presented fault will be formed and detected ms later and at a higher fault inception angle.

D. Wide area un-synchronized fault location.

The F1 can be accurately located by the FLU at the terminal of the 11kV substation bus (as shown in Fig. 10) due to the fact that no load branch is involved between the FLU and the fault point. These load branches although, have large impedances in the high frequency, can still absorb some of the high frequency transients. If multi-branches are placed in the fault loop the fault location may produce larger error. Using the wide-area measurement results from both of the source and the DG sides, this problem can be addressed.

Using the wide-area measured fault locations, the FLU (embedded in the DG protection) close to the fault gives the shortest fault location results. This result is most accurate duo to least branches included during the fault location. The second smallest and/or the third smallest values are used to eliminate the “fake” results which might show the same distance but on different branches. This is demonstrated in Table 1 for all the nine faults.

As shown in the Table 1, values in the bracket are the real fault distances and the “NA” indicates the fault located more than 10km from the FLUs and with more than four branches in between. For all the fault locators installed at the DG sides, the highlighted parts are the FLUs which have the shortest estimated distance to the fault and will give a more accurate result. However, for F1, the source side FLU will give a better result due to smaller source impedance and fewer branches between the fault the measurement point.

Table 1 Wide area fault location results for F1-F9

Fault	F1	F2	F3	F4	F5	F6	F7	F8	F9
FLU0 (kM)	10.01(10)	16.02(16.8)	21.61(17.4)	NA(19.7)	16.21(18.0)	NA(27.9)	NA(27.8)	NA(34.1)	NA(34.8)
FLU2 (kM)	1.44(1.5)	7.54(8.3)	5.11(5.9)	6.72(8.2)	6.31(6.5)	NA(16.4)	NA(24.8)	NA(31.1)	NA(23.3)
FLU5 (kM)	8.92(9.7)	NA(16.5)	2.09(2.3)	2.62(2.8)	NA(13.7)	14.22(11.0)	NA(19.4)	NA(25.7)	NA(15.1)
FLU8 (kM)	NA(16.9)	NA(23.7)	6.31(8.0)	4.11(4.4)	NA(13.7)	3.42(3.8)	15.38(12.2)	NA(18.5)	NA(22.3)
FLU11 (kM)	NA(22.1)	NA(28.9)	NA(13.2)	6.91(9.6)	NA(18.9)	1.29(1.4)	6.47(7.0)	16.32(13.2)	NA(27.5)
FLU15 (kM)	NA(34.2)	NA(41)	NA(25.3)	NA(21.7)	NA(31.0)	NA(13.5)	4.69(5.1)	1.07(1.2)	NA(39.6)
FLU17 (kM)	NA(41.7)	NA(48.5)	NA(32.8)	NA(29.2)	NA(38.5)	NA(21.0)	9.75(12.6)	6.02(6.3)	NA(47.1)
FLU18 (kM)	0.57(0.6)	5.94(6.2)	6.02(8.0)	NA(10.3)	NA(8.6)	NA(18.5)	NA(26.9)	NA(33.2)	NA(25.4)
FLU20 (kM)	7.01(7.7)	0.86(0.9)	NA(15.1)	NA(17.4)	NA(15.7)	NA(25.6)	NA(34.0)	NA(40.3)	NA(32.5)
FLU24 (kM)	14.5(12.2)	NA(19.0)	NA(16.6)	NA(18.9)	6.74(7.3)	NA(27.1)	NA(35.5)	NA(41.8)	NA(34.0)
FLU28 (kM)	NA(17.7)	NA(24.5)	13.5(10.3)	NA(10.8)	NA(21.7)	NA(19.0)	NA(27.4)	NA(33.7)	6.76(7.1)
FLU31 (kM)	NA(26.8)	NA(30.8)	NA(16.6)	NA(17.1)	NA(28.0)	NA(25.3)	NA(33.7)	NA(40.0)	0.79(0.8)

Beside the highlighted smallest results, the rest of the FLU results can be used to help selecting the faulted sections. For example, F2 is 0.9km to the DG connected to the node 20 (FLU20) and it can be a fault either on the "left" or "right" of the DG connection point. Then the second smallest result (FLU18) can be used to verify that the fault is on the "left" side (if it were on the "right" side, the FLU18 result is larger than 7.1km). If there are three lines connected to one node besides the DG (in case the dashed loop connection lines are used), the third shortest results can be used for identifying the faulted line section. For practical utilization the ratio of the estimated results with the smallest distance is used to indicate the distance differences and the faults all over the system are pre-studied. The fault location can be decided by comparing with the online measurement results with the pre-studied patterns to reduce the data processing time.

The impedance estimated based fault location will suffer from the change of the distribution topologies. The proposed method compares distances estimated from all the FLUs to located possible faulted area and then uses the smallest fault location result to decide the final fault position. Assuming the change of the distribution topologies results in a $\pm 5\%$ errors for each of the estimations, in this case, the faults placed close to the start and the end of the line section (about 5-10%, as F1) might be located as on the neighbor lines. When this occurs, disconnection of the located line will not clear the fault and the neighbor lines will have to be disconnected as well (enlarged fault location area).

As long as it is fault with fault current that is larger than the load current and a measureable fault transient, the proposed method will work. For faults between phases and the grounded faults, the only differences are the faulted loops and the measured voltages and the fault location results will be the same. If one (or more) of the FLUs (measurements) is lost this would not lead to totally wrong fault location results but would lead to an enlarged estimated fault location area (the faulted line and its neighbor lines might be isolated). Considering errors from the updated system parameters, faults placed close to the start and the end of the line section might cause enlarged estimated fault location area as well.

IV. Conclusions

This paper proposes a high frequency impedance measurement based fault location method which is suitable for system with the penetration of DGs. Short rectangular window which only includes 6ms fault transients is used to prevent the influence of the control loops which normally have a cascaded response time larger than 100ms. The high frequency impedance model of DFIG is provided and tested. The fault location results derived using this model indicate good accuracy. The influences of the fault resistance and fault inception angles are considered. Applying the proposed method in a practical distribution system with laterals, the wide-area measurement based method can be used. Due to the fact that the data synchronizing is not required, the proposed method has the potential of practical utilization.

V. Reference

[1] J.R. Aguero, "Applications of smart grid technologies on power distribution systems," IEEE PES Innovative Smart Grid Technologies (ISGT), pp. 1, 2012.

[2] S.S. Venkata and N. Hatziargyrlou,"Grid resilience elasticity is needed when facing catastrophes", IEEE Power & Energy Magazine, Vol.13 No.3, pp.16-20, May 2015.

[3] E. Pouresmaeil, M. Mehrasa and J. P. S. Catalão,"IEEEA Multifunction Control Strategy for the Stable Operation of DG Units in Smart Grids,"IEEE Trans. SMART GRID, VOL.6(2), pp. 598-607, Mar, 2015.

[4] T. Takagi, Y. Yamakoshi, J. Baba, K. Uemura and T. Sakaguchi, "A new algorithm of an accurate fault location for EHV/UHV transmission lines part I – Fourier Transformation method," *IEEE Trans. Power Apparatus and system*, vol.100, pp. 1316-1323, Mar. 1981.

[5] T. Takagi, Y. Yamakoshi, M. Yamaura, R. Kondow and T.matsushima, "Development of a new type fault locator using the one-terminal voltage and current data," *IEEE Trans. Power Apparatus and system*, vol.101, pp. 1116-1123, Aug. 1982.

[6] K. Srinivasan and A. St-Jacques, "A new fault location algorithm for radial transmission lines with loads," IEEE Trans. Power Del., vol. 4, no. 3, pp. 1676–1682, Jul. 1989.

[7] A. Girgis, C. Fallon, D. L. Lubkeman, "A fault location technique for rural distribution feeders," *IEEE Trans. Industry Applications*, vol.34 (29). pp.1170-1175. Dec. 1993

[8] R. H. Salim, M. Resener, A. D. Filomena, K. R. C. d. Oliveira, and A. S. Bretas, "Extended fault-location formulation for power distribution systems," IEEE Trans. Power Del., vol. 24, no. 2, pp. 508–516, Apr. 2009.

[9] S. J. Lee, M. S. Choi, S. H. Kang, B. G. Jin, D. S. Lee, B. S. Ahn, N. S. Yoon, H. Y. Kim, and S. B. Wee, "An intelligent and efficient fault location and diagnosis scheme for radial distribution systems," IEEE Trans. Power Del., vol. 19, no. 2, pp. 524–532, Apr. 2004.

[10] R. Das, "Determining the locations of faults in distribution systems," Ph.D. dissertation, Univ. Saskatchewan, Saskatoon, SK, Canada, 1998.

[11] M.S. Choi, S.J. Lee, D.S. Lee and B.G. Jin, "A New Fault Location Algorithm Using Direct Circuit Analysis for Distribution Systems," *IEEE Trans. Power Delivery*, vol. 19 (1), pp. 35-41, Apr 2004.

[12] R. Das, M. S. Sachdev, and T. S. Sidhu, "A technique for estimating locations of shunt faults on distribution lines," in Proc. IEEE Commun., Power, Comput. Conf. , 1995, pp. 6–11.

[13] H. Nouri and M. M. Alamuti, "Comprehensive Distribution Network Fault Location Using the Distributed Parameter," *IEEE Trans. Power Delivery*, vol. 26 (4), pp. 2154-2162, Oct 2011.

[14] J. M. Florez, V. B.Nunez and G. C. Caicedo, "Fault Location in Power Distribution Systems Using a Learning Algorithm for Multivariable Data Analysis," IEEE Trans. Power Syst., vol. 22, no. 3, pp. 1715–1721, July. 2007.

[15] J. Zhu, D. L. Lubkeman, and A. A. Girgis, "Automated fault location and diagnosis on electric power distribution feeders," IEEE Trans. Power Del., vol. 12, no. 2, pp. 801–809, Apr. 1997.

[16] G. M. España, J. Florez and H. V.Torres, "Elimination of Multiple Estimation for Fault Location in Radial Power Systems by Using Fundamental Single-End Measurements," *IEEE Trans. Power Delivery*, vol. 264(3), pp. 1382-1389, July 2009.

[17] M. M. Alamuti, H. Nouri, R. M. Ciric, and V. Terzija, "Intermittent Fault Location in Distribution Feeders." *IEEE Trans. Power Delivery*, vol. 27 (1), pp. 96-103, Jan 2012.

[18] Z. Galijasevic and A. Abur, "Fault location using voltage measurements," *IEEE Trans. Power Del.*, vol. 17, no. 2, pp. 441–445, Apr.2001.

[19] R. A. F. Pereira, L. G.W. Silva, M. Kezunovic, and J. R. S.Mantovani, "Improved fault location on distribution feeders based on matching during-fault voltage sags," *IEEE Trans. Power Del.*, vol. 24, no. 2, pp.852–862, Apr. 2009.

[20] T. Tayjasanant, C. Li and Wilsun Xu,"A Resistance Sign-Based Method for Voltage Sag Source Detection," *IEEE Trans. Power Del.*, vol. 20, no. 4, pp.2544-2551, Oct. 2005.

[21] S. Lotfifard, M. Kezunovic, and M. J. Mousavi, "Voltage sag data utilization for distribution fault location," IEEE Trans. Power Del., vol. 26, no. 2, pp. 1239–1246, Apr. 2011.

[22] M. Reddy, D. Rajesh, P. Gopakumar and D. K. Mohanta, "Smart Fault Location for Smart Grid Operation Using RTUs and Computational Intelligence Techniques," IEEE Trans. Smart Grid., vol. 8, no. 4, pp. 1260–1271, Dec. 2014.

[23] Y. Dong, C. Zheng and Mladen Kezunovic, "Enhancing Accuracy While Reducing Computation Complexity for Voltage-Sag-Based Distribution Fault Location," EEE Trans. Power Del., vol. 29, no. 1, pp. 251–260, Feb. 2014.

[24] M. Majidi, A. Arabali and M. Etezadi-Amoli, "Fault Location in Distribution Networks by Compressive Sensing," *IEEE Trans. Power Del.*, vol. 30, no.4, pp.1761-1769, Aug. 2015.

[25] M. Majidi, M. Amoli, and M. Fadali, "A Novel Method for Single and Simultaneous Fault Location in Distribution Networks," *IEEE Trans. Power Del.*, vol. 30, no. 6, pp.3368-3376, Nov. 2015.

[26] Z.Q. Bo, G. We1 ler, M.A. Redfern, "Accurate fault location technique for distribution system using fault-generated high-frequency transient voltage signals," IEE ProccGener Trunsm. Distrib., Vol.146. No.1 pp.73-80. Jan 1999

[27] R. Razzaghi, G. Lugrin, H. Manesh, C. Romero, M. Paolone, F. Rachidi, "An efficient method based on the electromagnetic time reversal to locate faults in power networks," *IEEE Transaction on Power Delivery*, Volume:28(3) , pp.1663-1673. 2013.

[28] D.W.P. Thomas and C. Christopoulos," Ultra-high speed protection of series compensated lines," *IEEE Trans. Power Delivery*, vol. 7 (1), pp. 139-145, Dec 1992.

[29] P. A. Crossley and P. G. Mclaren, "Distance Protection Based on Travelling Waves," IEEE Trans. Power Apparatus and system, vol.102, pp. 1714-1720, Aug. 1983.

[30] F. H. Magnago and Ali Abur, "Fault Location Using Wavelets," IEEE Transactions on Power Delivery, Vol.13(4),pp.1475-1480, Oct 1998

[31] A. Borghetti, M. Bosetti, M. D. Silvestro, C. A. Nucci and M. Paolone "Continuous-wavelet transform for fault location in distribution power networks: definition of mother wavelets inferred from fault originated transients," *IEEE Trans. Power Del*, vol. 23, pp. 380-388, May. 2008.

[32] P.F. Gale and B.Tech, "Cable-fault location by impulse-current method," IEE Proc Vol. 122 (4), pp.43-47,Apr 1975.

[33] F. Han, X. Yu, M. Dabbagh and Y. Wang, "Locating Phase-to-Ground Short-Circuit Faults on Radial Distribution Lines," *IEEE Trans. Industrial Electronics*, vol. 54 (3), pp. 1581-1590, Jul 2007.

[34] K. Jia, T. Bi, B. Liu ; E. Christopher, D.W.P. Thomas, and M. Sumner, "Marine Power Distribution System Fault Location Using a Portable Injection Unit" *IEEE Trans. Power Del*, vol. 32 (2), pp. 818-826, Dec 2014.

[35] K. Jia, E. Christopher, D. Thomas, M. Sumner and T. Bi, "Advanced DC zonal marine power system protection," IET Gener. Trans. Distrib.Vol. 8, Iss. 2, pp. 301–309, Feb. 2014

[36] Z. He, J. Zhang, W. Li, and X. Lin,"Improved Fault-Location System for Railway Distribution System Using Superimposed Signal, *IEEE Trans. Power Delivery*, vol. 25 (3), pp. 1899-1911, Jul 2010.

[37] J. J. Florez, R. A. Orozco and A.Bedoya-Cadena,"Fault location considering load uncertainty and distributed generation in power distribution systems," *IET Gener. Transm. Distrib.*, Vol. 9, Iss. 3, pp. 287–295 2015

[38] J. Ren, S. S. Venkata and E. Sortomme, "An Accurate Synchrophasor Based Fault Location Method for Emerging Distribution Systems," *IEEE Trans. Power Delivery*, vol. 29 (1), pp. 297-298, Feb 2014.

[39] S. M. Brahma, "Fault Location in Power Distribution System With Penetration of Distributed Generation," *IEEE Trans. Power Delivery*, vol. 26 (3), pp. 1545-1553, July 2011.

[40] P. Chen, V. Malbasa, Y. Dong and M. Kezunovic, "Sensitivity Analysis of Voltage Sag Based Fault Location With Distributed Generation," *IEEE Trans. Smart Grid*, vol. 6 (4), pp. 2098-2106, July 2014.

[41] N. Perera, A. D. Rajapakse and T. E. Buchholzer, "Isolation of Faults in Distribution Networks With Distributed Generators," *IEEE Trans. Power Delivery*, vol. 23 (4), pp. 1545-1553, Oct. 2008.

[42] J. Morren and S. W. H. de Haan, "Short-Circuit Current of Wind Turbines With Doubly Fed Induction Generator,"IEEE Trans on Energy Conversion, Vol. 22(1), pp.174-180, Mar 2007

[43] J. Hu, Y. He, Lie Xu and B. W. Williams, "Improved Control of DFIG Systems During Network Unbalance Using PI – R Current Regulators," IEEE Trans on Industrial Electronics, Vol. 56(2), pp.439-451, Feb 2009

[44] S. Tohidi, H. Oraee, M. R. Zolghadri, S. Shao and P. Tavner, "Analysis and Enhancement of Low-Voltage Ride-Through Capability of Brushless Doubly Fed Induction Generator," IEEE Trans on Industrial Electronics, Vol. 60(3), pp.1146-1155, Mar 2012

[45] W. Chen, D. Xu, N. Zhu and etc., "Control of Doubly-Fed Induction Generator to Ride-Through Recurring Grid Faults," IEEE Trans on Power Elect, Vol. 31(7), pp.4831-4846, July 2016

[46] Gilbert Strang and Truong Nyuyen, *Wavelets and filter banks*. Wellesley-Cambridge Press, December, 1996.

[47] IEEE PES Distribution System Analysis Subcommittee's Distribution Test Feeder Working Group, "IEEE 33 Node Test Feeder," Tech. Rep., September 2011.

APPENDIX

Table 1 Network parameters of the testing system

Node i	Node j	Line type	Line length (km)	Loads(L) or DGs capacity of Node j (kVA or kW)	Node i	Node j	Line type	Line length (km)	Loads or DGs capacity of Node j (kVA or kW)
0	1	1	10	100+j60(L)	16	17	6	1.7	500(DG)
1	2	1	1.5	500(DG)	1	18	2	0.6	500(DG)
2	3	1	1.1	120+j80(L)	18	19	2	5.3	90+j40(L)
3	4	1	1.2	60+j30(L)	19	20	6	1.8	500(DG)
4	5	2	2.9	500(DG)	20	21	6	3.2	90+j40(L)
5	6	3	1.8	200+j100(L)	2	22	5	1.5	200+j100(L)
6	7	4	2	200+j100(L)	22	23	2	3.1	420+j200(L)
7	8	5	3.4	500(DG)	23	24	2	3.1	500(DG)
8	9	5	3.5	60+j20(L)	5	25	1	0.6	200+j100(L)
9	10	4	0.6	45+j30(L)	25	26	1	0.9	60+j25(L)
10	11	4	1.1	500(DG)	26	27	2	3.7	60+j20(L)
11	12	2	5.1	60+j35(L)	27	28	2	2.8	500(DG)
12	13	6	2.4	60+j20(L)	28	29	1	1.5	200+j600(L)
13	14	2	2.1	60+j10(L)	29	30	2	3.4	150+j70(L)
14	15	5	2.5	500(DG)	30	31	6	1.4	500(DG)
15	16	6	5.8	60+j20(L)	31	32	6	1.5	210+j100(L)

Table 2 Line parameters

Line type	Resistance per unit length (Ω/km)	Reactance per unit length (Ω/km)
1	0.331	0.169
2	0.286	0.238
3	0.107	0.356
4	0.353	0.117
5	0.302	0.216
6	0.223	0.297